The pressure dependence of optical flame emission from space propulsion-relevant hydrogen combustion

Robert Stützer, Thomas Fiala** and Michael Oschwald**
*DLR – German Aerospace Center, Institute of Space Propulsion
Im Langen Grund 1, D-74239 Hardthausen, Germany
**Technical University of Munich
Arcisstraße 21, D-80333 Munich, Germany

Abstract

The frequently used oxygen-hydrogen-combustion has been investigated regarding the pressure dependence of its radiation. Two crucial spectral regimes – the ultraviolet and the blue emission bands – where examined and compared in order to evaluate its response to pressure values ranging from ambient conditions up to space propulsion relevant levels of 80 bar. Combustion pressures of up to 40 bar are realized using a lab-scale jet-flame burner. Higher pressures where reached in a research rocket combustion chamber. Using a high-resolution spectrograph, the OH* emission is shown in detail on a picometer scale. Furthermore, the pressure impact on the emissivity of the visible spectral regime is higher than on the ultraviolet OH* radiation. However, the latter is strongly influenced by self-absorption, thereby limiting the transparency of the flame. Interpretation of both types of flame radiation and their origins are given. Dynamic pressure measurements are compared with optical data from both 306 nm and 430 nm wavelength. A strongly synchronous behaviour between chamber pressure and emissivity is revealed for a sampling rate of 100 kHz. A resonance frequency of 950 kHz becomes evident for measurements of both photon wavelength regimes and pressure detection. Moreover, flame shape and spatial radiation behaviour for several pressure values is shown and analysed.

1. Introduction

The propellant combination oxygen-hydrogen is still the indispensable workhorse for space launch activities. Due to its enormous specific impulse it is widely used for lifting heavy payload into Earth orbits. Though the chemical reaction of the combustion process is sufficiently investigated for ambient and moderate pressure conditions, experiments on the O-H reaction under high pressure values are very scarce, regarding spectrally resolved flame emission. Since extreme pressure conditions inside a rocket combustion chamber are the predominant challenge for a stable and steady combustion as well as for the viability of the thruster itself, effort must be undertaken towards a better understanding of high-pressure characteristics of the hydrogen burning. The well-established UV-NIR optical spectrum of the O-H flame reveals a dominant emission in the ultraviolet regime around 300 nm [1][2]. Only minor radiation is emitted in the visible range under 1 bar conditions. Thus, the flame appears nearly invisible for the human eye. The overwhelming emission in the ultraviolet range has been investigated for ambient pressure conditions experimentally [3][4][6] as well as numerically [5][6] in great detail.

Regarding flame emission, the origin and source of the UV-band has been identified and investigated several decades ago. Relatively less is known about the visible and infrared spectral regime. Atomic emission lines of the UV-band [3] are used to determine flame temperature [7]. However, using flame emission of hydrogen combustion for pressure determination has not been conducted so far.

Besides spectroscopic measurements, imaging techniques are often used for heat release determination and localisation in hydrogen combustion. Nevertheless, highly turbulent flames impede correct data acquisition. Therefore, measurements in rocket combustors are often accompanied by obstacles that have to be considered when applying optical techniques. Single laser-pulse UV-Raman spectroscopy has been used for analysis of high pressure hydrogen-fuelled combustion in rocket applications as well [8].

With its intense photon emission, the OH radical is well-suited for optical flame investigations. Pressure-resistant combustion chambers with optical access allow the realisation of extreme pressure and temperature conditions. Ambient pressure experiments have been conducted using a lab-scale burner, operated by the TU-Munich group of

Robert Stützer, Thomas Fiala

Sattelmayer and Fiala *et al*. High-pressure experiments where conducted at the European research and technology test bench P8 of DLR Lampoldshausen in Germany [9]. Experiments on two rocket combustors delivered relevant data for several analyses. Combustion chamber A (BKA) was used for laser-ignition tests. The induced ignition-plasma and the subsequent combustion was optically analysed regarding the response of light emission on fast pressure changes. Combustion chamber D (BKD), on the other hand, delivered spectroscopic flame emission data for the pressure range between 40 and 80 bar.

2. Experimental

In order to analyse different spectral regimes of the hydrogen combustion for a broad range of pressure values, three experimental setups have been used. For flame emission measurements under high-pressure conditions, two model rocket combustors where applied. The combustion chamber BKA was modified for laser-ignition experiments and rapid optical sampling. Combustor BKD has a glass window optical access and was used for spectral measurements at pressures of up to 80 bar. These data are completed with results of a lab-scale burner setup for pressure values under 40 bar and laminar flame shapes. All three setups are described here.

2.1 Combustion chamber A (BKA)

Combustion chamber A is a cylindrical, segmented model rocket combustor (fig. 1). Its inner diameter is 50 mm wide and its nozzle measures 33 mm in diameter. Propellant feed takes place using a faceplate, made of 15 coaxial injectors. Each injector element consists of a centred LOX-post and an outer ring for the injection of gaseous fuel (gH2). The centre element on the injector plate serves as an arbitrary igniter but was disabled for this study. Table 1 lists the injection parameters of the propellants in use.
Five identical segments are consecutively mounted to define the chamber length and to carry dynamic pressure sensors in order to observe flame propagation and high-frequency instabilities. The nozzle segment is not equipped with sensors.

Table 1: Preset injection conditions for laser-ignition tests on cryogenic propellants using rocket combustor A (BKA).

	max. mass flow	calc. injection velocity	temperature at ignition
	[g/s]	[m/s]	[K]
oxygen[a]	600	10.6	110; 280
hydrogen[b]	150	1300	120—280
methane[b]	200	450	279—290

[a]liquid; [b]gaseous

Data used for this study have been sampled by sensors mounted on the diagnostic segment which is located directly at the mult-injector faceplate. Figure 2 depicts all relevant probes, sensors and the position of the laser-induced plasma spark. The optical probe is connected to photo-multiplier units in order to intensify and record photons, generated and emitted within the line-of-sight. The optical access was realised using sapphire rods, installed inside patent pending stainless steel probes (design: S. Gröning, DLR Institute of Space Propulsion), described elsewhere [10].
Ignition itself was triggered using a laser burst of 20 single laser pulses, fired with a frequency of 50 Hz, a pulse width of 1—2 ns, and a peak energy of 30 mJ. The applied laser-ignition system was a Q-switched HiPoLas® laser fabricated by CTR (Carinthian Tech Research AG) directly mounted to the combustion chamber via a lens tube containing optics for optimal focusing and precise focal point placing within the combustor. Furthermore, a Dalsa® Genie-HM 1024 surveillance camera was mounted in front of the nozzle with unobstructed view to the place of ignition. The camera possesses a monochromatic 2/3" CMOS sensor with global shutter and 1024 x 768 pixels. The sequence of interest was recorded with the maximum frame rate of 117 fps. A LED light source was installed behind

the camera to illuminate the combustion chamber face plate. Both camera and light source were encased inside a steel housing with a 2 cm thick quartz glass window on its front end. Convective cooling with gaseous nitrogen prevented the system from overheating when exposed to hot gases of the exhaust plume.

Using dynamic sensors with a sampling rate of 100 kHz, optical as well as pressure measurements were carried out to obtain highly time-resolved data. Probe port 1 for observation of the laser-induced plasma is connected to a photomultiplier that is equipped with an optical band-pass filter for 306 ± 5 nm, probe port 2 is linked to two spectrographs via split fiber optics, and probe port 3 delivers emission data via a photomultiplier equipped with a band-pass filter for 430 ± 10 nm. Thus, simultaneous sampling of pressure data and optical emission in the UV and visible (blue) regime are possible.
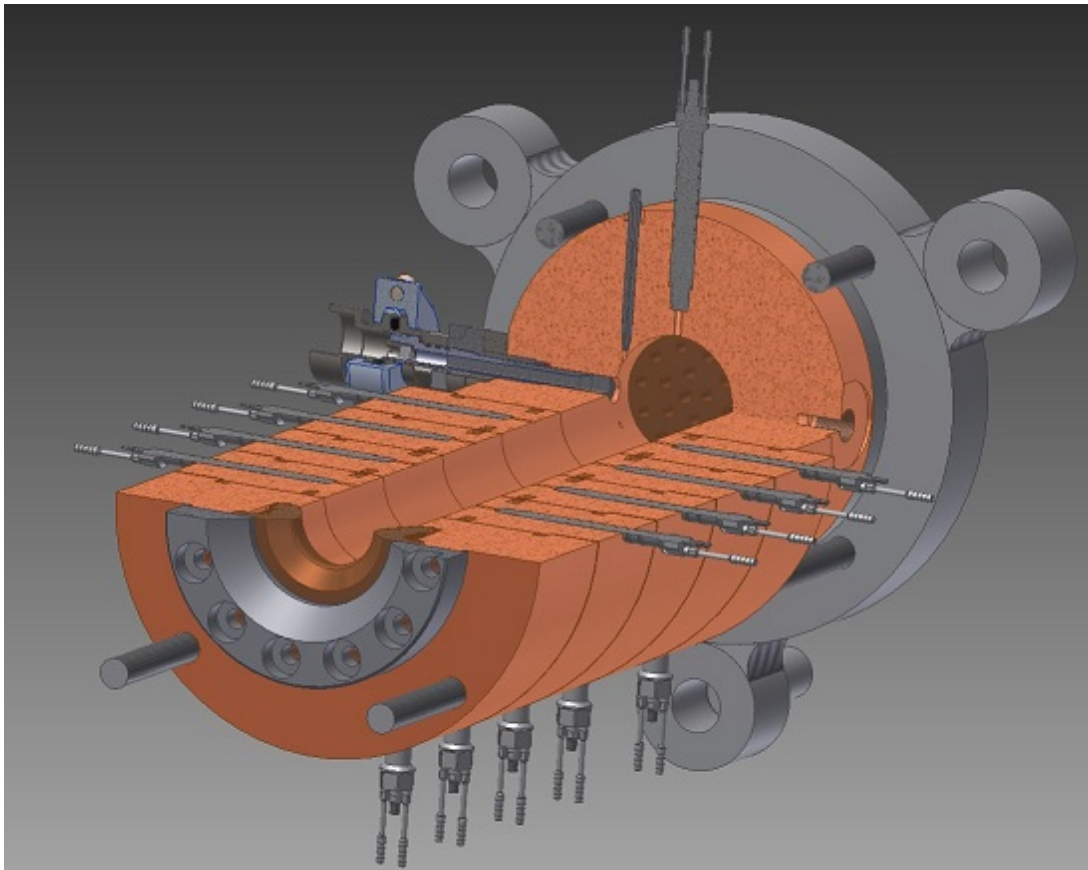
Figure 1: Cut away view of combustion chamber A (BKA).

2.2 Combustion chamber D (BKD)

The model research combustor D (BKD) [12,13] is a multipurpose subscale rocket combustor operated with the propellant combination hydrogen/oxygen at the P8 test facility at the DLR, German Aerospace Center. As shown in fig. 3 (left), BKD consists of three main elements: the injector head, the cylindrical combustion-chamber segment, and the nozzle segment. It has a chamber diameter of 80 mm and a nozzle-throat diameter of 50 mm. The injector head is equipped with 42 shear coaxial injectors. Oxygen is injected at supercritical pressures, and the operating conditions are representative of modern flight engines using the propellant combination hydrogen/oxygen.

For optical investigation, the measurement ring depicted in fig. 3 (right) is installed between the injector head and the cylindrical segment. It is equipped with the same fiber-optical probes as in BKA [10,13]. A small sapphire rod is mounted at the tip of the optical probe to create the optical access. Behind the sapphire rod, the radiation is captured by an optical fiber connected to a Czerny–Turner-type Princeton Instruments SP-2750 spectrometer (focal length: 750 mm) and recorded by a PI-MAX intensified camera (1024 × 256 active pixels, front illuminated, Peltier-cooled CCD). The fiber is a high-OH silica fiber with low attenuation in the UVand visible range. The full acceptance angle of the optical probes is approximately 2 deg. On the length scale of the combustion chamber, the field of view can be

Robert Stützer, Thomas Fiala

approximated as a line. For the test runs presented here, the spectrometer is connected to optical probe number 4, as shown in fig. 3 (right). It is aligned to an injector on the second ring of the injector pattern.
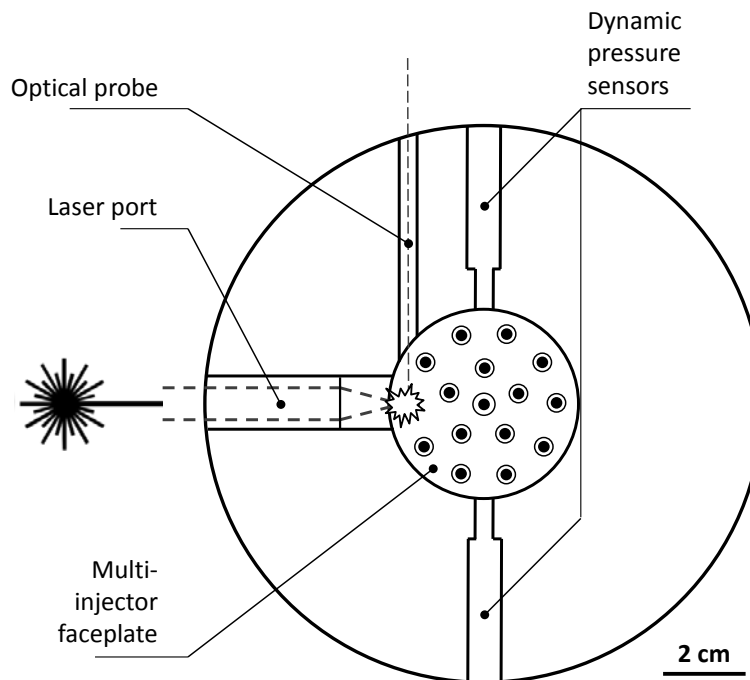
Figure 2: Diagnostic segment (front view) as used in combustion chamber A for optical and pressure measurements [11]. The laser-induced ignition spark is located at an outer coaxial injector with the possibility for plasma spectroscopy (LIBS).

In the presented work, the results of two test runs are used. In the first test run, the combustion-chamber pressure was varied in four steps of 10 bar from 80 to 50 bar. The oxidizer-to-fuel ratio was 5. The hydrogen temperature ranges between 114 and 122 K, and the oxygen temperature between 113 and 117 K. The load point of the second test run has a combustion-chamber pressure of 70 bar with an oxidizer-to-fuel ratio of 6.8. The average hydrogen temperature was 97 K and the average oxygen temperature was 123 K.

The test runs used different spectrometer configurations. For the first test run, a relatively coarse grating with a spacing of 150 grooves per millimeter was used to measure a wavelength range from 290 to 430 nm, including the OH* system as well as parts of the blue radiation. With this grating, the exposure time was set to 33 ms and spectra were recorded with a sampling frequency of 20 Hz. In the second test run, the structure of the OH* system was investigated in detail. The spectrometer was equipped with a fine grating with a spacing of 3600 grooves per millimeter. To achieve higher spectral resolution of the OH system, the measured wavelength range was reduced to the range between 305.1 and 310.2 nm. For this grating, a longer exposure time of 900 ms was required and spectra were recorded with a sampling frequency of 1 Hz. All spectral data are device function corrected and smoothed by moving average.

2.3 Combustion chamber H (BKH)

Research combustor H (BKH) has a rectangular cross section and five shear coaxial injection elements clustered centrally. A detailed description of BKH can be found elsewhere [14]. In the present work, the results will be presented from testing with per-element total mass-flow rates of 110—130 g/s, and with LOX and gH2 injected at temperatures of approximately 120 and 70 K, respectively. The chamber is designed to reach mean operating pressures of 40 and 60 bar. Optical-access windows allow the flame to be observed in the near-injection region. The optical setup relevant to the results presented in this work is illustrated schematically in the description of a similar arrangement tested previously [15]. One high-speed camera collects OH* emission via a dichroic mirror, band-pass

filter for λ= 310±5 nm, and intensifier. The second camera collects flame luminosity in the visible range. No filters are applied, and so the collected spectral content depends on the sensitivity of the CMOS sensor in the camera, which ranges from 400 to 900 nm, peaking at around 650 nm. This arrangement includes radiation from a broad wavelength range. The removal of OH* wavelengths through the use of a filter leads to a visible emission spectrum dominated by the contributions from the blue radiation. Consequently, visible imaging showcases the same qualities observed in the laminar-jet-flame experiment, but at conditions representative of rocket engines.
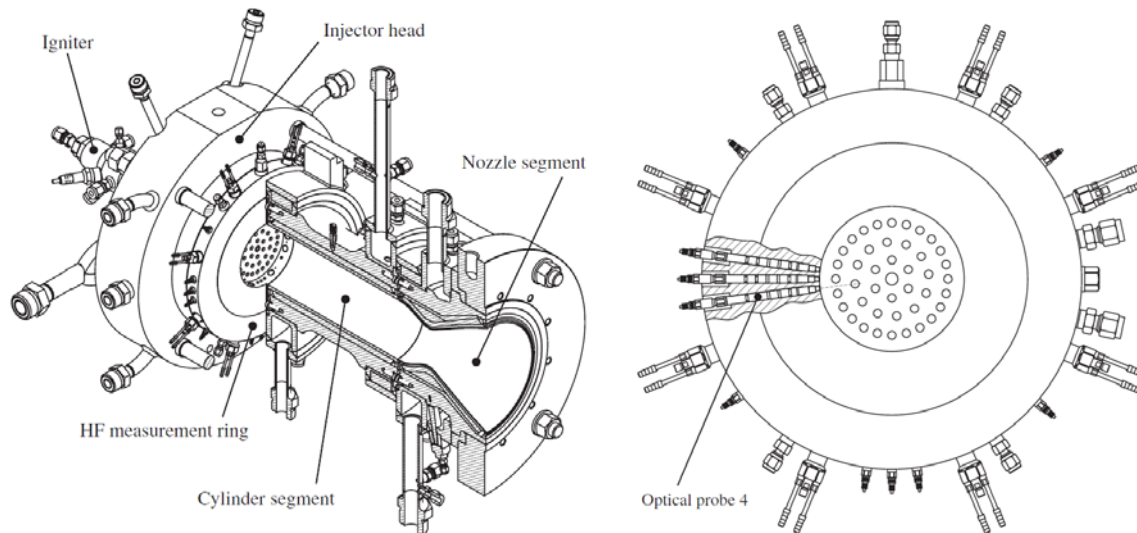
Figure 3: Research combustor BKD. Left: overview. Right: measurement ring.

2.4 Low pressure burner

In order to study a laminar jet flame under low pressure conditions, a low pressure burner had been developed and applied at the Technical University of Munich [16]. In addition to the detailed experimental investigation, flowfield simulations assessed the quality of the radiation modeling [17, 18]. As turbulent flames in rocket combustion are known to show flamelet character, these findings are assumed to represent the typically highly turbulent combustion in real rocket engines.

The flame is established by a jet of gaseous oxygen burning in hydrogen coflow (fig. 4). It is shielded by a round quartz tube to protect the flame from the ambient gas. The setup is enclosed in a pressurized vessel and operated at pressures up to 40 bar. Optical access is enabled by quartz windows at the side of the burner, through which the entire flame can be observed. An image-intensified camera is used to capture the flame radiation. In order to record the radiation of the $\Delta v= 0$ transition of the OH radical, a band-pass filter with a central wavelength of 308.5±5 nm is mounted in front of the UV camera lens. For the investigation of the blue radiation, a band-pass filter with a central wavelength of 456.270 nm and a FWHM of 2.370 nm is used instead. In addition to the recording of the flame's own radiation, a backlight from a 500 W Hg(Xe) lamp can be installed to study the flame's absorption.

The flowfield is simulated numerically using a commercial computational fluid dynamics (CFD) code. Models for predicting the band-pass-filtered OH* [17] and blue radiation [18] have been developed and applied. For further details of the setup and simulation, please refer to [19].

Robert Stützer, Thomas Fiala
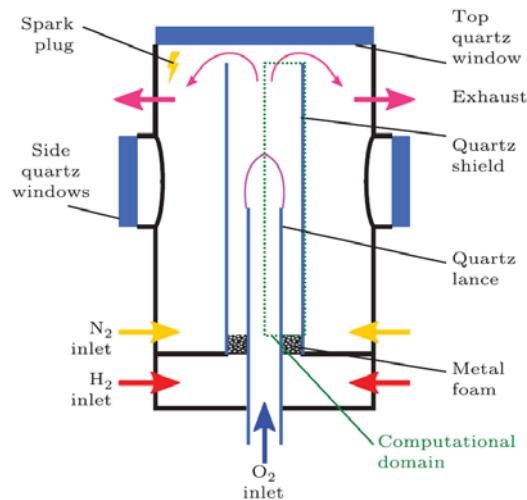
Figure 4: Sketch of the jet flame experiment in the low pressure burner [19].

3. Results and Discussion

Laboratory burner and model rocket combustors yield measurements of both OH* and blue radiation. Results of experiments on laminar and turbulent flames are shown and discussed here regarding time and spatially resolved radiance as well as spectral response.

3.1 Flame emission spectra

Unlike for emission spectra of atmospheric and low-pressure hydrogen-flames, which are readily available in the literature [1, 2], quantified data on high-pressure flames are sparse. Figure 5 (left) shows four emission spectra of the flame emission in BKD between pressures of 50 and 80 bar. The line-of-sight integrated measurements are from the first test run in BKD, as described in Sec. 2.2. Each of the four spectra consists of the average of 18 single exposures. The spectra show the familiar hydroxyl bands around 310 nm ($\Delta v = 0$) and 345 nm ($\Delta v = -1$), and traces of the 280 nm band ($\Delta v = 1$) are visible at the lower end of the recorded spectrum. The spectrum consists of numerous spectral lines. The measurement with the fine grating in test run 2 reveals the fine structure of between 306 and 309 nm as seen in fig. 5 (right). This figure also shows the calculated spectrum of a 0.5-mm-thick stoichiometric hydrogen-oxygen flame at 70 bar.
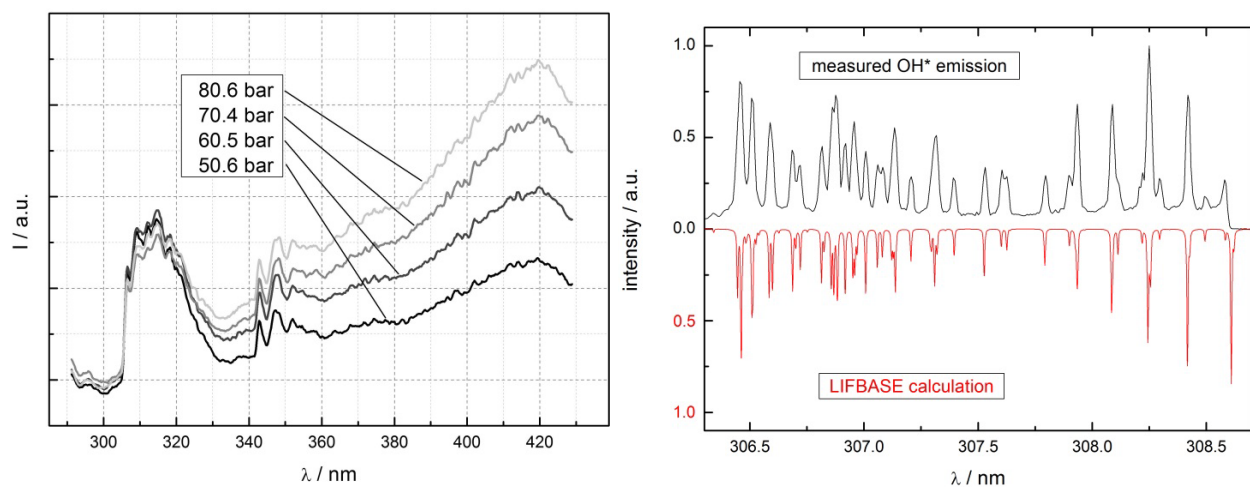
Figure 5: Left: Flame emission spectra from BKD at various pressure levels. Right: High-resolution emission spectrum of the UV regime as measured (black) and calculated using LIFBASE code (red).

The simulation is carried out using an object-oriented implementation of the HITRAN database [20] featuring self-absorption. The adiabatic flame equilibrium is computed from Cantera [21]. In general, the experimental and computed data show the same line position and intensity distribution. This excellent agreement demonstrates the ability for accurate optical measurements on relatively turbulent flames even at elevated temperatures.

The coarse spectrum in fig. 5 (left) also shows the spectrum of the blue radiation. Although weak in the UV, it becomes stronger with increasing wavelength. Its maximum value at 60 bar and above is higher than the peak of the OH* radiation. The spectrum is continuous and shows a reproducible fine structure, as reported earlier [22]. The blue spectrum appears to peak at 420 nm. However, the reduction toward a higher wavelength might be due to reduced sensitivity and, therefore, higher uncertainty at the edge of the detector range, and, thus, has to be treated with care. In the literature, the peak of the blue radiation is reported to be between 430 and 440 nm [1, 19].

The two different spectra respond very differently to changes in pressure. On one hand, the OH* radiance remains fairly insensitive to pressure. In contrast, the blue radiation increases significantly with pressure. It must be noted that the measurements are from a particular line of sight through the combustor. They do not represent the overall radiance, and cannot account for changes in flame shape or strain rate. Nevertheless, from direct comparison, it can be concluded that pressure has a stronger impact on the blue radiation compared to the OH* radiation.

At this point, the analysis is only preliminary because the probe volume is limited. Therefore, changes in flame topology could, in theory, also be the reason for the observed intensity variations. However, as will be shown, both blue and OH* radiations originate from the same region in the flame. Thus, the aforementioned conclusion is justified.

In general, the spectral measurements are in agreement with typical hydrogen-flame spectra at lower pressures [23]. However, the high-pressure levels investigated in this study reveal the strong increase of the blue radiation with pressure. This underlines the potential of the blue radiation as a flame marker for high-pressure measurements. In addition, the spectral comparison shows that OH* and blue radiation are very different. Whereas OH* shows a pronounced band spectrum with single identifiable spectral lines, the spectrum of the blue radiation is continuous.

3.2 Total radiance

The total flame radiance is a good scalar indicator to quantitatively discuss the influence of changes in operating conditions on the two types of radiation. Ideally, as the flame shape is altered by changes in operating conditions, recording of the entire flame radiation would be the most meaningful parameter. However, of the experiments investigated in this study, only the laminar jet flame provides optical access to the entire flame. For BKD and BKH, the radiance of a certain region of the flame will be examined.

In the case of the laminar jet flame, the total radiance is obtained by summing up the photon counts of the camera measurements with either band-pass filter installed. This is done for various pressure levels up to 40 bar. The total radiances of the jet flame are presented as a function of pressure in fig. 6. The abscissa is drawn in logarithmic scale to illustrate the strong increase of luminescence with pressure. Values above 35 bar have to be treated with care because the flame is flickering due to buoyancy at these operating conditions. This is also visible in the diagram, which presents the standard deviation of the various measurements as error bars.

For the OH* radiation, a strong increase is observed for low pressures. This is mostly due to the increase of flame temperature with pressure, which has an exponential impact in the following equation:

$$e_{\text{OH}^*} \sim [\text{OH}^*] \sim [\text{OH}] \cdot \exp\left(-\frac{hc}{k_B \lambda T}\right) \tag{1}$$

In addition, the concentration of ground-state OH, which also enhances OH* radiance, increases with the denser flame. However, due to buoyancy, the strain rate gradually increases and the flame becomes smaller. The reduction of luminous area leads to the stagnation of radiance. Furthermore, self-absorption prevents radiation originating from the back of the flame to reach the detector, thereby further reducing the total luminosity.

The total blue radiation shows a similar dependency on pressure. However, the increase is much stronger. Whereas OH* radiation is about 40 times stronger at 30 bar compared to atmospheric pressure, the blue radiation increases by a factor of more than 1000 between 1 and 40 bar. This behavior can be explained, if the blue radiation is assumed to originate from H2O2* chemiluminescence and reaction

$$[\text{OH}] + [\text{OH}] \rightarrow \text{H}_2\text{O}_2^* \tag{2}$$

is the dominating path of formation. The quadratic dependency of the emissivity on the OH concentration explains a stronger impact of flame density compared to the OH* radiation, which only linearly depends on the OH

concentration. The reduction of luminous area due to buoyancy straining similarly causes a reduction of radiation increase. However, the blue radiation appears to steadily increase over the entire range of pressures investigated. Obviously, the highly turbulent flame in BKD is very different from the laminar flame. Additionally, the BKD measurements are only from a single line of sight and do not represent the radiation of the entire flame. A direct comparison with the laminar flame data is, therefore, not possible. Nevertheless, a relative comparison between OH* and blue radiation for the elevated pressure range can be made. Whereas OH* radiation appears to remain at an approximately constant level between 50 and 80 bar, the blue radiation increases by a factor of approximately 2.

With BKH, the total OH* radiance was investigated for two operating pressures: 40 and 60 bar. The measurement of flame radiance is restricted to the window region.
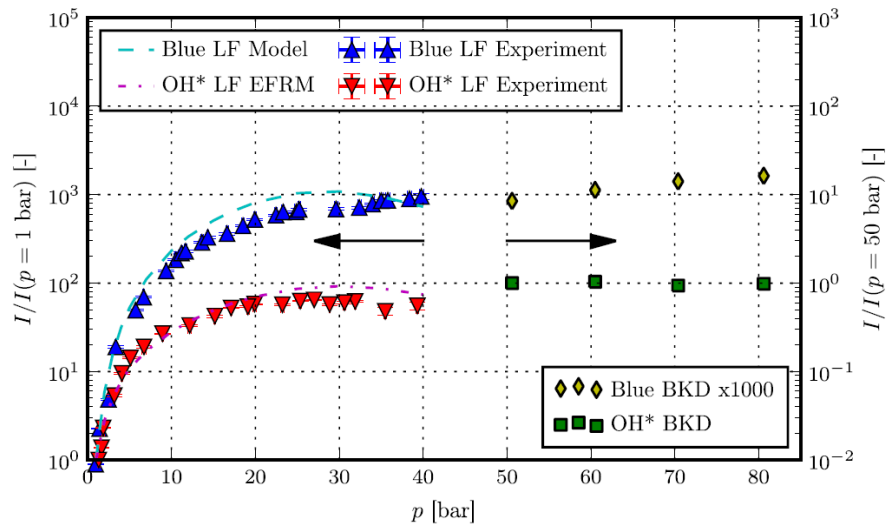
Figure 6: Total/average blue and OH* radiations (LF = laminar flame) [16].

3.3 Dynamic radiance

In order to investigate the capabilities of OH* and blue radiation to capture dynamic phenomena, highly time-resolved simultaneous measurements are carried out in combustor BKA. This study focuses on the data provided by the sensors installed at probe locations 1 and 3 of fig. 2. The attached fiber at probe port 1 is equipped with an optical band-pass filter for 306 ± 5 nm. Its line of sight intersects with the focus point of a laser used for ignition. Therefore, it detects both flame emission and radiation of the plasma decay. Probe port 3, on the other hand, is equipped with an optical band-pass filter for 430 ± 10 nm to evaluate the blue regime of the flame emission. Unlike probe port 1, probe port 3 is not aligned for plasma detection.

The results of the optical measurements are shown exemplarily in figs. 7 a—d. Synchronous pressure data are depicted in figs. 7 e—f for comparison. The left-hand side of fig. 7 shows traces of the temporal signals and on the right-hand side of fig. 7 traces of the temporal signal are displayed. At t = 0.075 s, only the pressure-sensor data show an abrupt increase, indicating the beginning of injection. The distinct radiation peaks at t < 0.0005 s in the OH* signal derive from the laser-induced plasma emission, which can only be detected via probe port 1 due to its line-of-sight intersection with the plasma cloud. Although the first six laser pulses create plasma breakdown, no ignition takes place, probably due to the absence of LOX in the combustion chamber. Only gH2 can be spectrally detected until 0.2 s after t0 [11]. The seventh laser pulse causes a highly noisy signal indicating the presence of combustion. Approximately 2.25 s after t0, the optical and pressure sensors drop to a minimum value because combustion has ceased. After the last laser pulse, the OH* emission intensity somewhat decreases, but then rises again after 0.51 s. Between 0.6 and 1.75 s, the ultraviolet emission retains at a relatively constant but noisy level. In contrast, the flame emission of the optical regime around 430 nm rises continuously following ignition until 1.75 s. Unlike the OH* signal, the blue-radiation signal does not dip toward zero during the course from ignition to engine shutdown. Both optical data as well as the pressure values reached their maximum 2 s after ignition. After engine shutdown, the optical emission abates to zero and the pressure decreases to 2.5 bar due to subsequent purging.
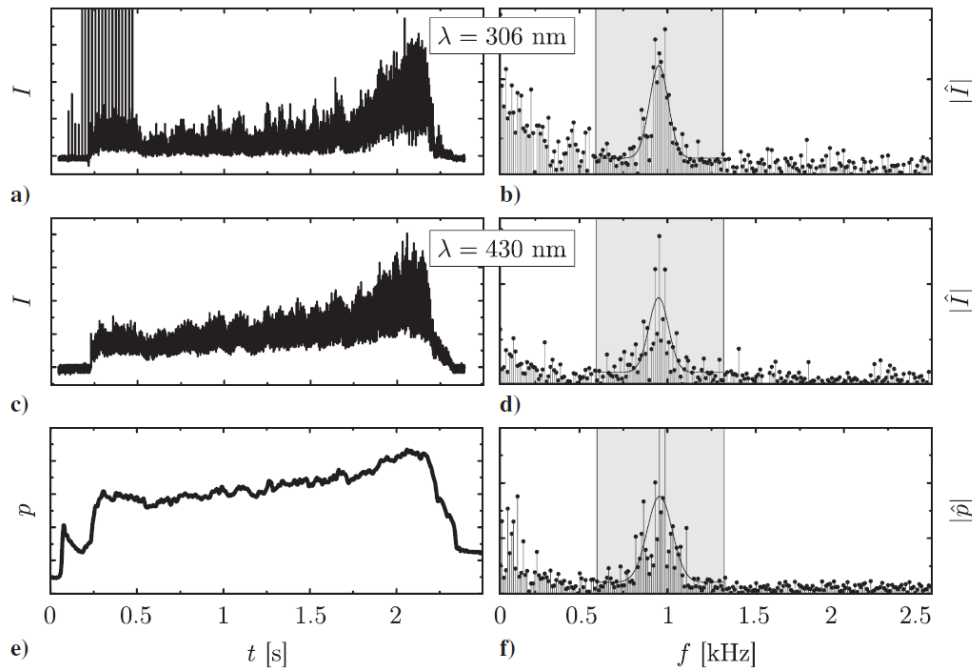
Figure 7: Dynamic sensor data (left) and the corresponding FFT analysis (right) in BKA.

To reveal combustion disturbances, a frequency analysis of the dynamic data is carried out using a Fast Fourier Transform (FFT) algorithm with a rectangular window function for the time domain of quasi-steady-state combustion. The results are depicted in figs 7 b, d and f. Both optical and pressure measurements show the same frequency response with a characteristic peak at the combustor eigenfrequency around 960 Hz and the same half-width of approximately 190 Hz, determined by Lorentzian fit. This shows the consistency between the dynamic-pressure measurements and the optical data of both wavelength regimes. However, the noticeable difference between the optical and pressure data is the relatively noisy character of the former and a comparatively steady distribution of the latter. The highly turbulent combustion, which by itself takes place at a very broad frequency spectrum and thus influences emission and absorption, is the source of the optical noise. The pressure fluctuation is directly governed by the geometrical field. Therefore, it exhibits the corresponding eigenfrequency more pronounced.

4. Conclusion

Two optical flame emission regimes have been investigated and compared: The intense OH* radiation in the ultraviolet regime as well as the blue radiation of the hydrogen-oxygen combustion. For the latter, the physical source is still unknown, but studies indicate that it originates form chemiluminescence reaction (2) forming excited hydrogen peroxide. In this study, the OH* and blue radiations are analyzed and compared with data obtained from four different test rigs. Spectrally, the two types of radiation are very different. Whereas the OH* radiation shows a banded spectrum with distinct spectral lines, the blue radiation exhibits a very broad, continuous spectrum. Except from very-high-pressure levels, their overlap below 310 nm is small, such that the two types of radiation can be distinguished using optical band-pass filters. The OH* and blue radiations are also different in terms of self-absorption. Particularly, hydrogen–oxygen flames at high pressures have a high concentration of ground-state hydroxyl (OH). At high pressures, a significant proportion of the OH* radiation is absorbed, essentially making the flame opaque. In contrast, no self-absorption was observed for the blue radiation. With respect to this type of radiation, the flames are optically thin. Additionally, pressure has a higher impact on the blue radiation compared to the OH* radiation.

Both types of radiation are also suitable for the validation of numerical simulations. The high temperature simplifies the simulation of OH* to thermal-equilibrium calculations. However, absorption has to be accounted for in high-pressure situations. For line-of-sight integrated radiation simulations, the blue radiation is preferable. Because of its square dependency on the OH concentration, the turbulence–radiation interaction is less important compared to for

OH*. However, as there is up to now only one validation for the blue radiation model in the literature, it still has to be verified for broader use.

References

[1] Gaydon, A. 1974. Spectroscopy of Flames. Chapman & Hall Ltd.

[2] Mavrodineanu, R., and H. Boiteux. 1965. Flame Spectroscopy. John Wiley & Sons, Inc.

[3] Dieke, G., and H. Crosswhite. 1962. The Ultraviolet Bands of OH. *J. Quant. Spectrosc. Radiat. Transfer.* 2:97—199.

[4] Parigger, C., G. Guan, and J. Hornkohl. 2003. Measurement and analysis of OH emission spectra following laser-induced optical breakdown in air. *Applied Optics.* 42:5986—5991.

[5] Hall, J., and E. Petersen. 2006. An Optimized Kinetics Model for OH Chemiluminescence at High Temperatures and Atmospheric Pressures. Wiley Periodicals, Inc.

[6] Brockhinke, A., J. Krüger, M. Heusing, and M. Letzgus. 2012. Measurement and simulation of rotationally-resolved chemiluminescence spectra in flames. *Applied Physics B.* 107:539—549.

[7] Pellerin, S., J. Cormier, F. Richard, K. Musiol, and J. Chapelle. 1996. A spectroscopic diagnostic method using UV OH band spectrum. *J. Phys. D: Appl. Phys.* 29:726—739.

[8] Wehrmeyer, J., R. Osborne, and H. Trinh. 2001. Measuring rocket engine temperatures with hydrogen Raman spectroscopy. *NASA Technical Report.*

[9] Haberzettl, A. *et al.*. 2000. European research and technology test bench P8 for high-pressure liquid rocket propellants. In: *36th AIAA/SAE/ASME/ASEE Joint Propulsion Conference.*

[10] Gröning, S. *et al.*. 2015. Analyses of Phase Shift Between Oscillations of Pressure and Flame Radiation Intensity of Combustion Instabilities. In: *6th European Conference for Aeronautics and Space Sciences (EUCASS).*

[11] Stützer, R., Börner, M., and Oschwald, M., 2015. Optical Investigation of a Laser-Ignited Cryogenic Rocket Combustion. In: *6th European Conference for Aeronautics and Space Sciences (EUCASS).*

[12] Suslov, D., Woschnak, A., Sender, J., and Oschwald, M.. 2003. Test Specimen Design and Measurement Technique for Investigation of Heat Transfer Processes in Cooling Channels of Rocket Engines Under Real Thermal Conditions. In: *39th AIAA/ASME/SAE/ASEE/JPC Conference and Exhibit.* 4614.

[13] Gröning, S., Hardi, J., Suslov, D., and Oschwald, M.. 2016. Injector-Driven Combustion Instabilities in a Hydrogen/Oxygen Rocket Combustor. *Journal of Propulsion and Power.* 32:560—573.

[14] Hardi, J. 2012. Experimental Investigation of High Frequency Combustion Instability in Cryogenic Oxygen-Hydrogen Rocket Engines. *Ph.D. Thesis.* School of Mechanical Engineering, University of Adelaide, Adelaide, Australia.

[15] Webster, S., Hardi, J., and Oschwald, M. 2014. High Pressure Visualisation of Liquid Oxygen and Cryogenic Hydrogen Combustion Under an Imposed Acoustic Field. In: *Proc. of the 19th Australasian Fluid Mechanics Conference.* Edited by Chowdhury, H., and Alam, F., Australasian Fluid Mechanics Society, Melbourne, p. 153.

[16] Fiala, T., Sattelmayer, T., Gröning, S., Hardi, J., Stützer, R., Webster, S., and Oschwald, M. 2017. Comparison Between Excited Hydroxyl Radical and Blue Radiation from Hydrogen Rocket Combustion. *Journal of Propulsion and Power.* 33:490—500.

[17] Fiala, T., and Sattelmeyer, T. 2016. Assessment of Existing and New Modeling Strategies for the Simulation of OH* Radiation in High-Temperature Flames. *CEAS Space Journal.* 8:47—58.

[18] Fiala, T., and Sattelmeyer, T. 2016. Modeling of the Continuous (Blue) Radiation in Hydrogen Flames. *International Journal of Hydrogen Energy.* 41:1293—1303.

[19] Fiala, T., 2015. Radiation from High Pressure Hydrogen-Oxygen Flames and its Use in Assessing Rocket Combustion Instability. *Ph.D. Thesis.* Technical University of Munich, Munich, Germany.

[20] Rothman, L., Gordon, I., Barbe, A., Benner, D., Bernath, P., Birk, M. Boudon, V., Brown, L., Campargue, A., Champion, J.-P., Chance, K., Coudert, L., Dana, V., Devi, V., Fally, S., Flaud, J.-M., Gamache, R., Vandaele, A., and Auwera, J. *et al.* 2009. The HITRAN 2008 Molecular Spectroscopic Database. *Journal of Quantitative Spectroscopy.* 110:33—572.

[21] Goodwin, D., Moffat, H., and Speth, R. 2015. Cantera: An Object-Oriented Software Toolkit for Chemical Kinetics, Thermodynamics, and Transport Processes, Ver. 2.2.0. www.cantera.org.

[22] Schefer, R., Kulatilaka, W., Patterson, B., and Settersten, T. 2009. Visible Emission of Hydrogen Flames. *Combustion and Flame.* 156:1234—1241.

[23] Diederichsen, J., and Wolfhard, H. 1956. Spectrographic Examination of Gaseous Flames at High Pressure. In: *Proc. of the Royal Society of London, Series A: Mathematical, Physical and Engineering Sciences.* 236:89—103.